

Non-redundant odor coding by sister mitral cells revealed by light addressable glomeruli in the mouse

Ashesh K Dhawale^{1,2}, Akari Hagiwara³, Upinder S Bhalla², Venkatesh N Murthy³ & Dinu F Albeanu¹

Sensory inputs frequently converge on the brain in a spatially organized manner, often with overlapping inputs to multiple target neurons. Whether the responses of target neurons with common inputs become decorrelated depends on the contribution of local circuit interactions. We addressed this issue in the olfactory system using newly generated transgenic mice that express channelrhodopsin-2 in all of the olfactory sensory neurons. By selectively stimulating individual glomeruli with light, we identified mitral/tufted cells that receive common input (sister cells). Sister cells had highly correlated responses to odors, as measured by average spike rates, but their spike timing in relation to respiration was differentially altered. In contrast, non-sister cells correlated poorly on both of these measures. We suggest that sister mitral/tufted cells carry two different channels of information: average activity representing shared glomerular input and phase-specific information that refines odor representations and is substantially independent for sister cells.

The responses of neurons in a sensory circuit depend on the interaction between direct input received from sensory afferents, lateral input from neurons in the same circuit, as well as feedback from other brain areas. In mammals, olfactory sensory neurons (OSNs) send their axons to the olfactory bulb, where there is a characteristic physical layout of inputs at the glomerular layer¹. Each glomerulus receives convergent afferents from a large number of OSNs expressing the same odorant receptor^{2,3}. The principal neurons in the olfactory bulb, the mitral and tufted (mitral/tufted) cells, typically have only one primary dendrite that projects to a single glomerulus. A few dozen mitral/tufted cells share input from the same parent glomerulus¹. Mitral/tufted cells also receive lateral GABAergic and dopaminergic inputs from a variety of interneurons in the glomerular and external plexiform layers¹, thus allowing them to sample information from several functionally diverse glomeruli.

To what extent is the output of mitral/tufted cells shaped by the input from the parent glomerulus versus lateral signals originating from other glomeruli in the bulb? Do mitral/tufted cells that have their primary dendrites in the same glomerulus, referred to as sister cells, carry redundant information about odors to higher brain centers? Progress in answering these questions about redundancy and the topography of lateral connectivity has been slowed by the nature of odor representations at the input layer and the anatomy of the bulb. Activating individual input elements (glomeruli) selectively is difficult because individual odors tend to activate distributed populations of glomeruli^{4,5} and not all glomeruli can be activated, even with a large palette of odors⁶.

We developed new tools for activating glomeruli optically with high spatial and temporal precision. We engineered transgenic mouse lines that express the light-activated ion channel channelrhodopsin-2 (ChR2)⁷

specifically in OSNs. Then, using a digital mirror device (DMD) to deliver patterned light stimulation onto the olfactory bulb in conjunction with extracellular recordings, we obtained the glomerular receptive field maps of individual mitral/tufted cells. By identifying the parent glomeruli, we were able to directly examine the similarity of odor responses of sister and non-sister mitral/tufted cells.

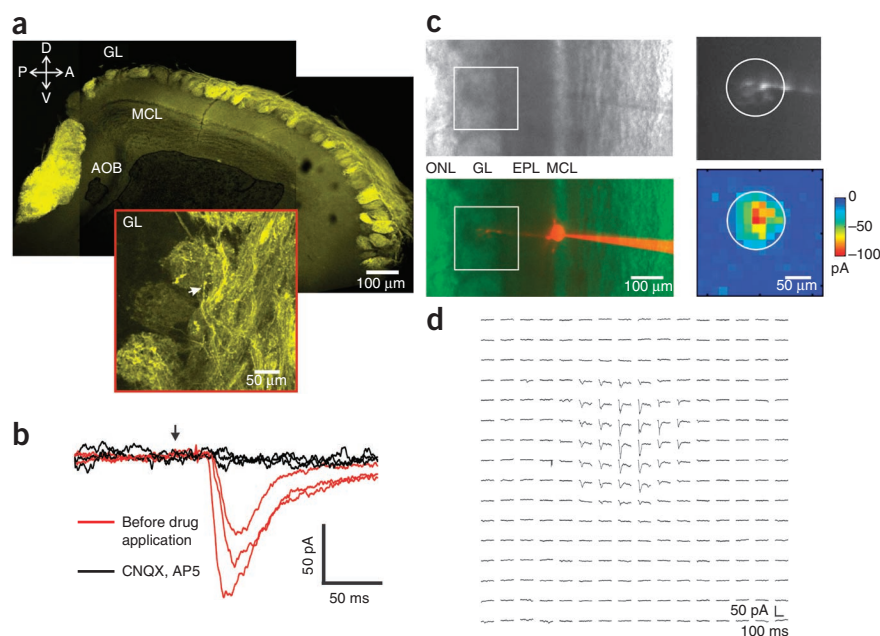
RESULTS

We generated transgenic mice that express ChR2-EYFP (enhanced yellow fluorescent protein) in all mature OSNs using the *olfactory marker protein* (*Omp*) promoter (ORC mice), such that all glomeruli were light sensitive (Fig. 1a). We characterized the ORC mice *in vitro* using acute brain slices and laser-scanning photostimulation⁸. Whole-cell patch clamp recordings from mitral cells (Fig. 1b,c) showed reliable light-evoked currents only in response to photostimulation of the glomerular layer. These responses were blocked by ionotropic glutamate receptor antagonists 6-cyano-7-nitroquinoxaline-2,3-dione (CNQX) and D(-)-2-amino-5-phosphonovaleric acid (AP5) ($n = 5$ cells; Fig. 1b–d). Furthermore, when stimulating at subglomerular inter-foci spacing (15 μm), excitatory currents (Fig. 1d) were obtained by stimulation of only a single glomerulus for each recorded cell (Fig. 1c). Fluorescent dye (Alexa 546) loaded into the recorded mitral cell confirmed that its apical dendrite projected to the same glomerulus whose stimulation evoked currents (Fig. 1c). Increasing the stimulation intensity led to larger currents (Supplementary Fig. 1), as well as to a spread of the hotspot to areas adjacent to the input glomerulus (Supplementary Fig. 1), presumably as a result of activation of ChR2 in axons of passage. These results confirm that activation of ChR2 in olfactory sensory axons in single glomeruli could depolarize their terminals effectively, causing glutamate release to activate postsynaptic neurons.

¹Cold Spring Harbor Laboratory, Cold Spring Harbor, New York, USA. ²National Centre for Biological Sciences, Tata Institute of Fundamental Research, Bangalore, India. ³Department of Molecular and Cellular Biology, and Center for Brain Science, Harvard University, Cambridge, Massachusetts, USA. Correspondence should be addressed to V.N.M. (vnmurthy@fas.harvard.edu) or D.F.A. (albeanu@cshl.edu).

Received 14 July; accepted 24 September; published online 17 October 2010; doi:10.1038/nn.2673

Figure 1 ORC transgenic expression pattern. Laser-scanning photostimulation identified parent glomeruli for mitral cells in ORC mice olfactory bulb slices. **(a)** Confocal micrograph of olfactory bulb sagittal section from ORC mice showing EYFP fluorescence. A, anterior; AOB, accessory olfactory bulb; D, dorsal; GL, glomerular layer; MCL, mitral cell body layer; P, posterior; V, ventral. Scale bar represents 100 μm . Inset, higher magnification view, arrow indicates OSN axons. Scale bar represents 50 μm . **(b)** Bath application of glutamate receptor antagonists CNQX and AP5. The three traces for each of the conditions correspond to three adjacent photostimulation foci 50 μm apart (red trace, before drug application; black trace, during drug application; arrow indicates the time of photostimulation). **(c)** Phase (top left) and red fluorescence image (bottom left) of one mitral cell filled with Alexa 546; the box indicates the field of photostimulation. Top right, primary dendrite and tuft projecting to a glomerulus. Bottom right, matching 2DLAM (16×16), inter-foci distance = 15 μm , photostimulation duration = 1 ms. Note the fiduciary circle on the two panels. Color represents the peak amplitude of the light-induced currents. ONL, olfactory nerve layer. Scale bar represents 100 μm . **(d)** Currents recorded in the mitral cell by laser-scanning photostimulation in **c** are shown at locations corresponding to each point in the 16×16 grid. Traces were averaged across four repeats, 1.6-mW laser power was used. Scale bars represent 50 pA and 100 ms.



Identification of parent glomeruli of mitral/tufted cells by light

We adapted a DMD from a commercial digital light projection (DLP) projector (see Online Methods) to construct an instrument that allowed us to illuminate the olfactory bulb surface with arbitrary light patterns (at ~ 470 nm, see Online Methods) and photo-activate glomeruli *in vivo* (Fig. 2). Thus, we were able to optically control neuronal activity at subglomerular resolution, with each pixel on the DMD corresponding to a ~ 5 - μm spot on the bulb surface.

We simultaneously recorded mitral/tufted cell activity using tetrodes that were inserted at a depth of 250–300 μm in the olfactory bulb of anesthetized ORC mice (Online Methods). The surface of the bulb was tessellated into a square grid and each square pixel was illuminated sequentially by single focal spots of light in a pseudo-random spatial order (Fig. 2a). The stimulating light spots were of the same size or smaller (20–75 μm) than the average mouse glomerulus (~ 75 μm)^{6,9}. Light stimulation induced rapid and reliable changes in firing, peaking at 25–50 ms and lasting for 100 ms on average (Fig. 2b).

For each single unit (Fig. 2c) satisfying our selection criteria (Online Methods), we constructed a two-dimensional light activation map (2DLAM) at subglomerular resolution (75 μm down to 20 μm ; Fig. 2c and Online Methods). The light intensity was successively lowered until no light-triggered activity was seen in any unit being recorded (down to intensities lower than 2 mW mm⁻²). This ensured that we were operating in the regime of minimal glomerular activation (Fig. 2d) with negligible nonspecific activation of axons of passage, as observed in acute slice experiments.

Because any given mitral/tufted cell in the adult mouse olfactory bulb receives excitatory inputs from only one glomerulus¹, we interpreted the hotspots to be parent glomeruli for the corresponding mitral/tufted cells. This was supported by the observation that reducing light levels led to a single hotspot on the 2DLAMs for all 40 units that were light responsive. In addition, the average size of the hotspot at the lowest intensity of stimulation (73.6 ± 3.9 μm , $n = 40$) was comparable to the size of the average mouse glomerulus (74.2 ± 1.2 μm), as measured

in OMP-synaptotHluorin (OMP-spH) mice¹⁰ (572 glomeruli and 9 hemibulbs; Fig. 2e), consistent with anatomical studies⁹. Furthermore, taking advantage of YFP expression in glomeruli, we overlaid functional hotspots ($n = 9$) obtained from light mapping onto multiphoton z stack projections of images of YFP glomeruli taken in the same animal (Online Methods). The hotspots colocalized well with anatomical glomeruli (Fig. 3a and Supplementary Fig. 2) and the full width at half maximum (FWHM) of the hotspots fitted in the anatomical boundaries of matching glomeruli (Fig. 3b). Furthermore, the jitter between the centroids of hotspots and anatomical glomeruli was substantially smaller than the corresponding glomerular widths (Fig. 3c and Online Methods). The parent glomerulus for each isolated mitral/tufted unit was thus identified optically, just as it was done *in vitro*.

Glomeruli are generally laid out in a single row on the bulb surface, but occasionally they can be stacked on top of each other. As it could affect the correct assignment of parent glomeruli to mitral/tufted units, we quantified the frequency of this over-stacking. Multiphoton z stacks of ORC and OMP-spH glomeruli obtained via the same surgical configuration used for the physiology experiments revealed that only $\sim 6\%$ of glomeruli overlapped on the dorsal surface ($5.94 \pm 0.45\%$, 558 glomeruli, 4 ORC-M hemibulbs; $6.02 \pm 1.16\%$, 875 glomeruli, 7 OMP-spH hemibulbs; Fig. 3d and Supplementary Fig. 2).

Identification of sister and non-sister mitral/tufted cells by light

Using tetrodes or dual-tetrodes¹¹, we recorded odor responses simultaneously from multiple mitral/tufted units with defined parent glomerular identities. On average, we were able to isolate ~ 4 single units per recording site. We compared all possible pairs of light-responsive units obtained at each recording site ($n = 35$ pairs) by taking the difference of 2DLAMs corresponding to each unit (Fig. 4a–d). In some pairs, the hotspots were clearly spatially separated (Fig. 4b), whereas in others they were overlapping (Fig. 4d). Thus, some units appeared to receive inputs from different neighboring glomeruli (Fig. 4b), whereas others shared the same glomerular territory (Fig. 4d).

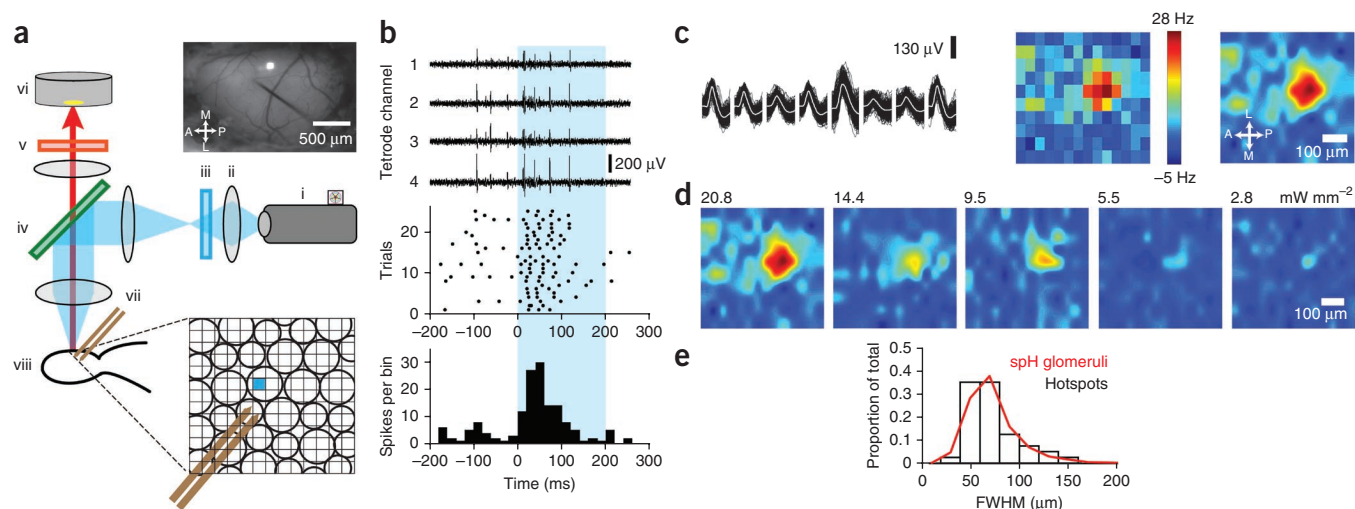


Figure 2 DMD patterned illumination in ORC mice maps the parent glomeruli of mitral/tufted cells *in vivo*. (a) Left, schematic of the DLP projector-based photostimulation setup. Top right, dorsal surface of the bulb with a tetrode positioned in the mitral cell layer. One square light spot can be seen projected onto the bulb surface. Scale bar represents 500 μm. Inset, cartoon schematic of glomeruli showing a subglomerular size light spot and dual-tetrodes positioned in the mitral cell layer. i, DLP projector; ii, focusing lens; iii, blue excitation filter; iv, dichroic mirror; v, emission filter; vi, CCD camera; vii, dual-tetrode; viii, olfactory bulb. (b) Top, raw voltage traces corresponding to the four channels of a tetrode during photostimulation. Center, raster plot of spikes from an isolated single unit. Bottom, peri-stimulus time histogram (PSTH) with 20-ms time bins. (c) Left, example spike waveform of a single unit across the eight channels of a dual-tetrode. Dark traces represent individual spikes and the white line represents the average waveform. Center, 2DLAM showing the change in firing rate of the mitral/tufted unit during photostimulation over ten repeats. Scale bar represents 100 μm (light spot size, 50 μm). Right, 2DLAM re-sampled by interpolation. (d) 2DLAMs obtained at different stimulation intensities (spot size, 50 μm). All maps were normalized to the highest bin in the 20.8 mW mm⁻² 2DLAM. (e) Distribution of 2DLAM hotspot widths (FWHM) for all units ($n = 40$) obtained in a minimal photostimulation regime (black bars). The distribution of synaptophluorin-labeled glomerular widths (FWHM) from OMP-spH mice (red line, $n = 572$) is shown.

We needed an objective criterion for classifying the recorded mitral/tufted units as sister cells or non-sister cells (Fig. 4e). For each pair, we calculated the Euclidean distance between the centers of the hotspots, normalized by the mean width (FWHM) of the two hotspots considered (Fig. 4f). We found that the size of glomeruli was greater than or equal to one FWHM of the functional hotspots (Figs. 2e and 3a–c). Therefore, pairs of mitral/tufted units whose parent glomeruli were

placed less than one mean FWHM apart were classified as being sister cells and the rest as being non-sister cells. Two distinct populations emerged (Fig. 4f) that were unambiguously separated by the FWHM criterion. Out of the 35 mitral/tufted pairs that we considered, 20 were found to be sisters. In a second strategy, we computed the correlation between the 2DLAMs for each mitral/tufted pair (Supplementary Fig. 3 and Supplementary Note 1); this approach yielded the same

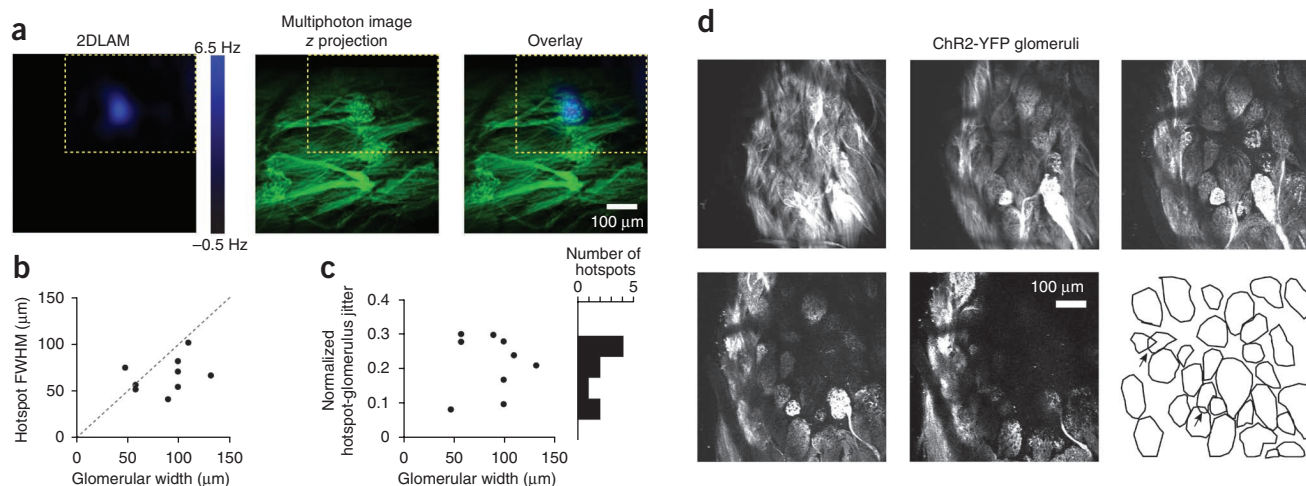


Figure 3 Functional hotspots correspond to anatomically identified glomeruli. (a) Left, functional hotspot from representative 2DLAM. Center, z stack image projection of anatomical glomeruli from the same field of view as the 2DLAM obtained via multiphoton microscopy. Right, overlay of the 2DLAM and the z projection. Yellow dotted lines indicate the boundaries of the 2DLAM. (b) Hotspot FWHMs plotted against corresponding anatomical glomerular widths. (c) Normalized spatial jitter between the centroids of functional hotspots and the corresponding anatomical glomeruli plotted against anatomical glomerular widths. The spatial jitter was normalized by the mean width of the anatomical glomerulus and the hotspot (a value of 1 corresponds to jitter of 1 glomerular width). (d) Example z stack image projections of OMP-ChR2-YFP glomeruli obtained via multiphoton microscopy. Each image shown is a 20-μm thick projection, taken 20 μm apart in the z axis from the subsequent one. Drawing illustrates contours of the glomeruli in the field of view. Arrows indicate overstacked glomeruli.

Figure 4 Light mapping sorts mitral/tufted cells into sister and non-sister pairs. **(a)** Example spike waveforms on individual tetrode channels for two isolated non-sister mitral/tufted cell units. **(b)** 2DLAMs for the units shown in **a** at different light intensities used for stimulation. The color scale to the right of the highest intensity maps indicates the range of firing rate changes with respect to baseline. All light maps for a particular unit are scaled to this range. Difference map refers to the difference between the normalized 2DLAMs of the two units, plotted for each of the light intensities used. Spatial scale bar represents 100 μm . **(c)** Example waveforms for two isolated sister mitral/tufted cell units. **(d)** 2DLAMs for the units shown in **c** at different light intensities used for photostimulation. The color scale is as described in **b**. The spatial scale bar represents 100 μm . **(e)** Cartoon schematic of parent glomerular connectivity for sister and non-sister mitral/tufted cells. **(f)** Separation of mitral/tufted cells into sisters and non-sisters based on Euclidean distance between the centers of light hotspots on 2DLAMs obtained in a minimal photostimulation regime. The distance between the centers of hotspots is expressed in units of the mean full width at half maximum (FWHM) of Gaussian fits to the two hotspots for each pair. Dotted line marks the separation between sister and non-sisters mitral/tufted cells and is placed at 1 FWHM.

results. The high proportion of sister pairs is a result of two factors: heterogeneity in light excitability of glomeruli and pre-selection bias to overcome the intrinsically low chance (20–30%) of recording sister pairs (**Supplementary Note 1**). We conclude that the physical separation between 2DLAM hotspots can be used to determine which mitral/tufted units share input from the same parent glomerulus.

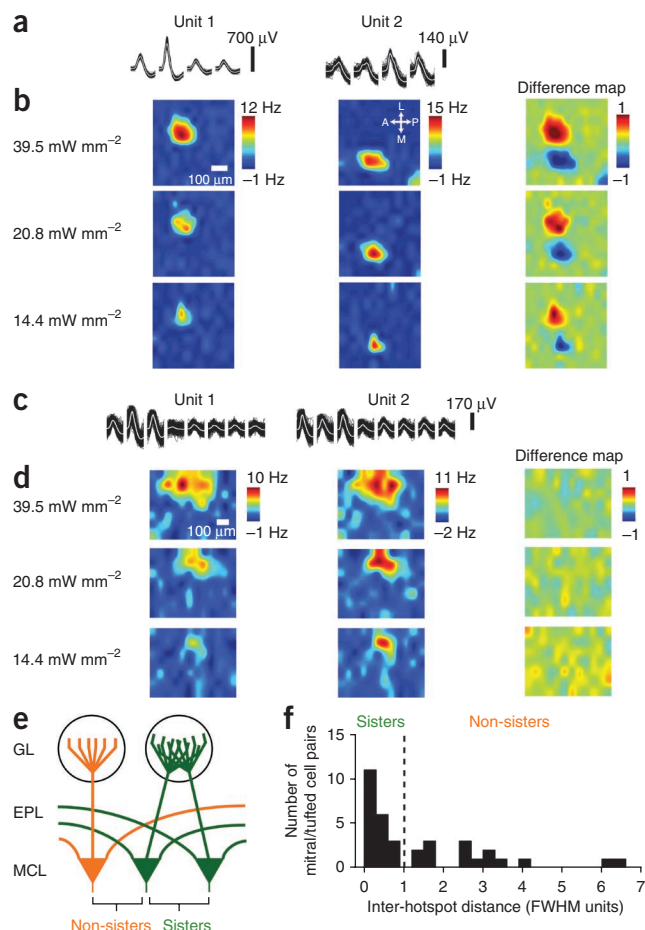
Odor response diversity in sister mitral/tufted cells

We next investigated the odor response properties of these mitral/tufted unit pairs to a set of 42 odor stimuli. Mitral/tufted firing is often locked to respiration¹² (**Fig. 5a,b**); that is, mitral/tufted cells tend to spike preferentially at a particular phase of the respiratory cycle. In response to an odor, mitral/tufted cell firing rates can increase or decrease from resting values and the timing of spikes in relation to respiration can be altered^{13–15}. We divided each cycle of respiration into five bins and populated these bins with spikes (**Fig. 5b,c**). The resulting vector, referred to as the phase tuning curve, was obtained for each mitral/tufted unit separately for the air period and odor period across many respiratory cycles (**Fig. 5b,c**) for all 42 odors. For example, one unit spiked reliably at the beginning and toward the end of the respiratory cycle during fresh air, but shifted its phase preference to a different point in the cycle, and underwent a reduction in firing rate once allyl-tiglate was presented (**Fig. 5a,b**).

Responses to multiple odors were compared in simultaneously recorded sister mitral/tufted cells (**Fig. 5c**). p-anis aldehyde increased the firing rates of both units, with odor-triggered spikes occurring at all phases of the respiratory cycle. For heptanal, however, the firing rate increased for unit 1, but was suppressed for unit 2. In response to 2-heptanone, although both units increased their firing rates, the phases of the respiratory cycle at which they predominantly spiked were different. Thus, we observed similarities and differences in the odor responses of sister mitral/tufted cells.

Odors induce correlated firing rate changes in sister cells

For each mitral/tufted unit, we calculated the average change in firing rate on odor presentation for all 42 stimuli and constructed a firing rate-based odor response spectrum (F-ORS; **Fig. 6a,b**, see Online Methods). Sister mitral/tufted units tended to be similar in their firing rate changes (**Fig. 6a**), as quantified by the Pearson correlation coefficient between the F-ORSs (0.68 ± 0.05 , $n = 20$; **Fig. 6c,d**). In contrast, the F-ORSs of non-sister pairs were



diverse (**Fig. 6b**) and had lower correlations (0.23 ± 0.11 , $n = 15$, $P = 2.4 \times 10^{-4}$, two-sample unpaired *t* test; **Fig. 6c,d**).

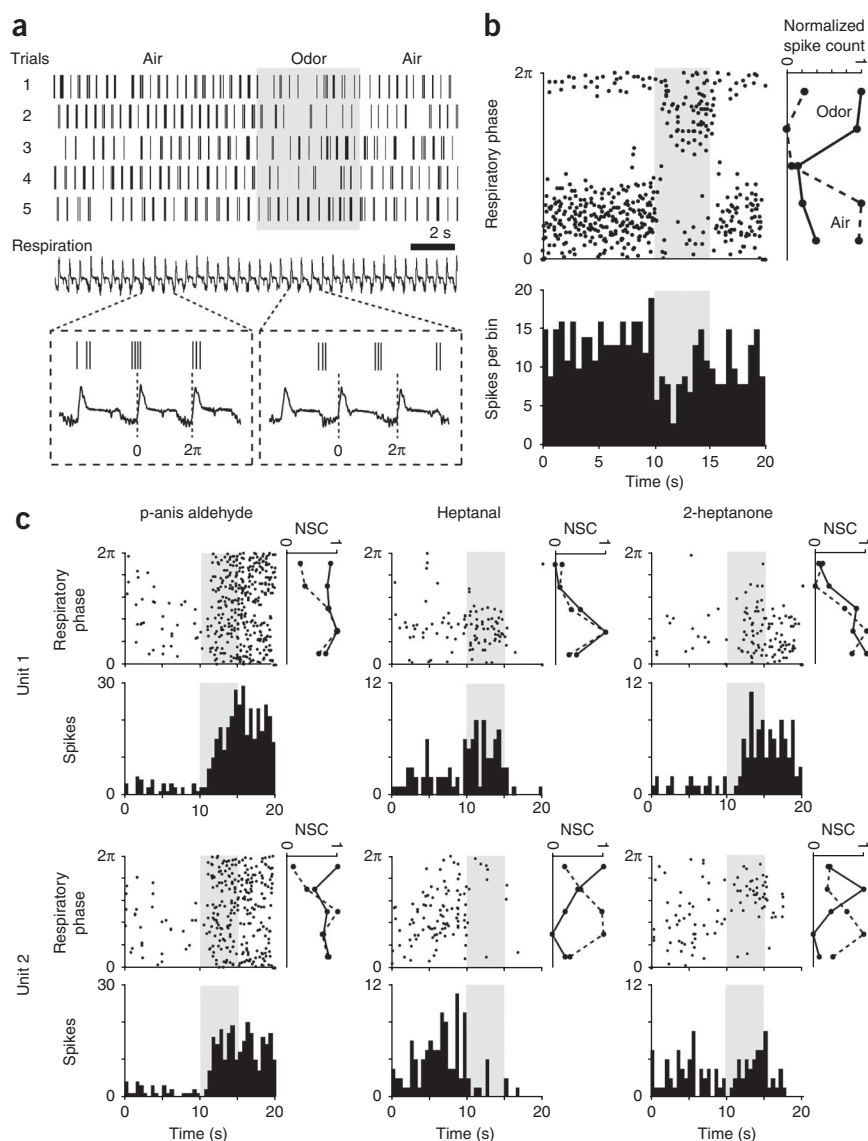
To obtain a measure of reliability for individual units across different trials, we split the odor repeats and calculated 'self' F-ORS correlations, whose average value was 0.67 ± 0.04 ($n = 40$). Sister pairs' F-ORS and self correlations were not significantly different ($P = 0.81$, also true when using a matched number of trials, data not shown). However, some odors did trigger different changes in the firing rates of sister cells (**Figs. 5c** and **6a**).

Sister mitral/tufted cells are desynchronized by odors

For each mitral/tufted cell, we constructed phase tuning curves during air and odor periods (**Fig. 7a**) for all stimuli. As a measure of similarity, we computed the correlation coefficient between the phase tuning curves in air and odor periods for each stimulus. We termed this the phase response, analogous to a firing rate response. The phase responses for all 42 odors then yielded a phase odor response spectrum (P-ORS; **Fig. 7b**) for each cell. For a given stimulus, a high value of the phase response (close to 1) indicates that odor presentation did not cause a substantial change in the phase tuning curve compared to the preceding air period.

How similar are phase responses for sister and non-sister pairs? We found that for sister pairs the average P-ORS correlation was only 0.18 ± 0.07 ($n = 20$; **Fig. 7c**), higher than, but not significantly different from, the average correlation for non-sister pairs (0.05 ± 0.06 , $n = 15$, $P = 0.16$). These low correlation values were not the result of a lack of reproducibility of phase response spectra across trials, as 'self' P-ORS correlation was 0.61 ± 0.05 ($n = 40$), which is significantly

Figure 5 Examples of similarities and differences in odor responses of sister mitral/tufted cells. **(a)** Example odor response of a mitral/tufted unit. Top, five odor stimulation trials are shown for this unit; vertical lines mark the time of a spike occurrence. Shaded area indicates the odor presentation window (5 s). Bottom, respiration trace. One respiratory cycle (labeled 0 to 2π) was typically ~500 ms long. Inset, expanded traces showing three respiratory cycles during air and odor presentation periods for one trial. **(b)** Top, phase-time plot of the odor response of the same mitral/tufted unit in **a**, shown over five repeats of allyl tiglate. Note the change in the preferred phase during odor stimulation (shaded area). To the right of the phase-time plot are phase tuning curves calculated during air (dotted line) and odor (continuous line) presentation in which each respiratory cycle was divided into five time bins. Bottom, PSTH of the same unit showing a drop in firing rate triggered by odor onset (bin width, 500 ms; NSC, normalized spike count). **(c)** Example odor responses to p-anis aldehyde, heptanal and 2-heptanone for two sister mitral/tufted cells (unit 1 and unit 2) shown as phase plots, PSTHs and phase tuning curves as in **b**. Left, note the strong increase in firing, spread across all respiration cycle phases for both units. Center, the excitatory versus inhibitory response triggered by odor onset in the two units. Right, the change in preferred phase of unit 2 triggered by the odor onset.



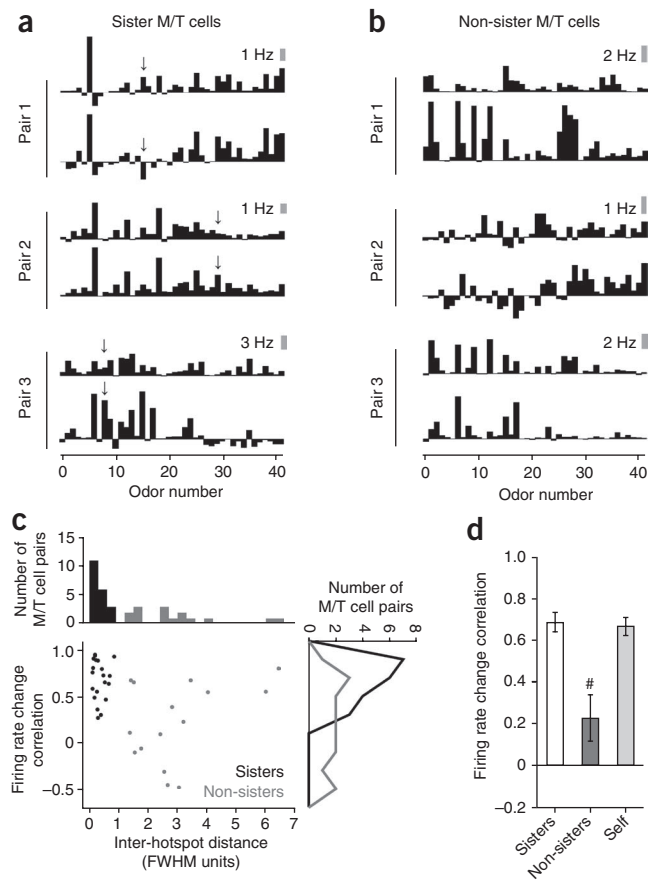
higher than both sister and non-sister P-ORS correlations ($P < 10^{-5}$ and $P < 10^{-7}$, respectively). Thus, unlike in the case of firing rate changes described above (Fig. 6), odors induce differential phase responses in both sister and non-sister mitral/tufted pairs.

How do odors induce distinct phase responses in sister cells? Do they start with similar phase tuning curves that diverge on odor stimulation or do they start with different phase tuning curves even at rest (air period)? To determine the phase relationship between units, we calculated the correlation coefficient between the phase tuning curves of the two units of a mitral/tufted pair, for all stimuli used. We calculated this inter-unit phase similarity (PS) separately for air and odor periods (Fig. 7d). Over the entire population of sister mitral/tufted cells, the average phase similarity for all stimuli was high during air and was significantly reduced when odors were presented (average $PS_{\text{air}} = 0.45 \pm 0.02$, average $PS_{\text{odor}} = 0.27 \pm 0.02$; $n = 20$ pairs times 42 odors, $P < 10^{-7}$, two-sample Kolmogorov-Smirnov test; Fig. 7d–f). This drop in phase similarity on odor presentation was not a result of a lack of reproducibility of phase tuning curves across trials, as the self phase similarity was high in both air and odor conditions (average self $PS_{\text{air}} = 0.45 \pm 0.01$, average self $PS_{\text{odor}} = 0.45 \pm 0.01$; $P = 0.05$, two-sample Kolmogorov-Smirnov test; Fig. 7f). Non-sister pairs had a broad, polymodal distribution of phase similarities at rest (air), with modes at positive and negative similarity values (Fig. 7e), clearly different from the distribution of sister pairs ($P = 0.004$, two-sample Kolmogorov-Smirnov test). This implies that different pairs of non-sister units fired consistently with different phase lags. Odor presentation flattened the distribution of phase similarity between the non-sister mitral/tufted units (Fig. 7e).

We obtained similar results if we focused on just the mean firing phase instead of the entire phase tuning curve for each stimulus (Supplementary Fig. 4 and Supplementary Note 2). We also examined the spiking relationship (Supplementary Fig. 5 and Supplementary Note 3) between pairs of mitral/tufted units with the more commonly used spike time correlation analysis. This analysis indicated that odor presentation led to significant broadening of the peak and a drop in peak height of the mitral/tufted units' auto-correlograms, as well as of sister pairs' cross-correlograms (Supplementary Fig. 4). Closer inspection revealed periodic modulation of spike timing in the beta and gamma frequency range for some mitral/tufted pairs, as seen previously¹⁶ (Supplementary Fig. 6), but on average we did not detect substantial power in these bands via coherence measurements at a population level (Supplementary Note 4). The odor-induced drop in phase similarity observed between sister units did not depend on the quality of unit isolation, the width of their hotspots or the distance between them (Supplementary Figs. 7 and 8 and Supplementary Note 5).

Odorants tend to activate multiple glomeruli. To investigate the effects of activating only the parent glomerulus on the phase properties of sister mitral/tufted pairs, we used the minimal light-stimulation strategy (Figs. 2 and 4) to modulate activity of single glomeruli

Figure 6 Sister mitral/tufted cells have correlated changes in odor induced firing rates. (a,b) Examples of F-ORSs obtained using a set of 42 odors for three pairs of sister (a) and three pairs of non-sister mitral/tufted (M/T) cells (b). Arrows in a denote differential responses across pairs of sister units. (c) A scatter plot of the similarity (correlation coefficient) of odor-induced firing rate change against the Euclidean distance between the centers of the hotspots in the 2DLAMs for each pair of mitral/tufted units that we considered. Gray indicates non-sister mitral/tufted cells and black indicates sister mitral/tufted cells. The marginal distributions are shown as histograms on the top and right axes. Top, separation of units into sister and non-sister mitral/tufted cells, as shown in Figure 3f. Right, histograms of sister ($n = 20$) and non-sister pairs ($n = 15$) F-ORS correlations. (d) Average F-ORS correlations for sister and non-sister mitral/tufted cells; self refers to the same unit ($n = 40$) probed across different blocks of odor repeats by splitting the total number of trials in two. $^{\#}P < 0.05$ for F-ORS correlations, across groups with respect to sister mitral/tufted pairs (for example, sister versus non-sister mitral/tufted units). Error bars represent s.e.m.



(Online Methods), by presenting light pulses continuously for 200-ms periods. As expected, light activation of individual glomeruli significantly increased the firing rate of sister mitral/tufted units compared to baseline (average 2.63 ± 0.47 Hz in the air period versus 9.10 ± 0.72 Hz in the light period, $P < 0.001$ by two-sample paired t test). The phase similarity between sister pairs was indistinguishable between air and light conditions (average $PS_{\text{air}} = 0.43 \pm 0.14$, average $PS_{\text{light}} = 0.42 \pm 0.12$, $n = 20$ pairs, $P = 0.88$, two-sample Kolmogorov-Smirnov test; Fig. 7g,h), even in instances in which light stimulation changed the phase preference of the sister mitral/tufted units (Fig. 7g).

These data indicate that sister mitral/tufted units are entrained by respiration to fire synchronously at rest, but become desynchronized (in terms of their firing relation to respiration) by odors. However, light activation of just the parent glomerulus altered the phase properties of sister units in similar manner. Non-sister mitral/tufted units fired with consistent phase lags with respect to each other when at rest. On odor stimulation, these predictable phase relationships were also disrupted.

Odor-induced firing rate and phase changes are independent

Are the differential firing rate and phase responses in sister mitral/tufted units (Figs. 6 and 7) that we observed caused by the same odors? To answer this question, we identified odors that affected one unit in a distinct manner compared with the other (Online Methods).

More odors had differential effects on phase than on firing rate in sister pairs ($18.7 \pm 3.0\%$ versus $9.3 \pm 2.3\%$ of odors, $P = 0.02$, Wilcoxon signed-rank test, Fig. 8a), as anticipated (Figs. 6 and 7). Notably, the percentage overlap between odors that caused differential responses in firing rate and phase was $1.6 \pm 0.6\%$, not different from chance ($1.4 \pm 0.5\%$, $P = 0.68$, by Wilcoxon signed-rank test; Fig. 8a and see Supplementary Note 6). For non-sister mitral/tufted pairs, similar percentages of odors caused both firing rate and phase similarity changes ($19.1 \pm 3.9\%$ versus $18.1 \pm 5.4\%$), also overlapping only to chance levels ($P = 0.95$, Wilcoxon signed-rank test). It is noteworthy that similar percentage of odors caused a decrease in phase similarity for sister ($18.1 \pm 3.0\%$) and non-sister pairs ($19.1 \pm 3.9\%$, $P = 0.51$, two-sample Kolmogorov-Smirnov test).

These results indicate that odors can induce differential changes in the phase of sister mitral/tufted cells without inducing differential changes in firing rates. Thus, changes in phase and firing rate are independent.

DISCUSSION

We engineered transgenic mice with optically excitable glomeruli, which offer many possibilities for dissecting the circuitry of the early

olfactory system. We used these mice to identify sister mitral/tufted cells and found that their odor responses are not redundant.

Optical activation of inputs to the olfactory bulb

The expression of ChR2 in the OSNs provides unprecedented control over glomeruli, the elementary input units of the bulb. This is an important advance in the study of olfaction, as it has been difficult to selectively activate every glomerulus in a region with odors. This approach could be extended to map the 'surround' for each mitral/tufted neuron, uncovering glomeruli that provide inhibitory input and thus obtain the glomerular receptive field for each mitral/tufted cell, which has not been possible until now¹⁵. Beyond circuit mapping, these mice could also be used for behavioral studies to test hypotheses about odor coding and perception^{17,18}.

The ORC mouse contrasts with the Thy1-ChR2 mouse¹⁹, which expresses ChR2 in a large fraction of mitral/tufted cells. Light control of neuronal activity in these Thy-1 ChR2 mice bypasses the first level of processing and is agnostic to important transformations on the inputs that take place in the glomerular layer, including feedforward inhibition^{20,21}. The two transgenic lines are likely to provide complementary information on circuits in the olfactory bulb.

The DMD patterned illumination strategy that we adapted has been employed extensively in vision research²², as well as to control neuronal activity in other systems²³. In comparison to laser-scanning photostimulation, DMDs can stimulate multiple foci in parallel to deliver a range of stimuli—from single spots to spatio-temporally complex natural (odor like) or even arbitrary activity patterns. Finally, different stimulation wavelengths can be easily co-projected to trigger excitatory and inhibitory responses in parallel, for multi-color control of neuronal circuits^{24,25}.

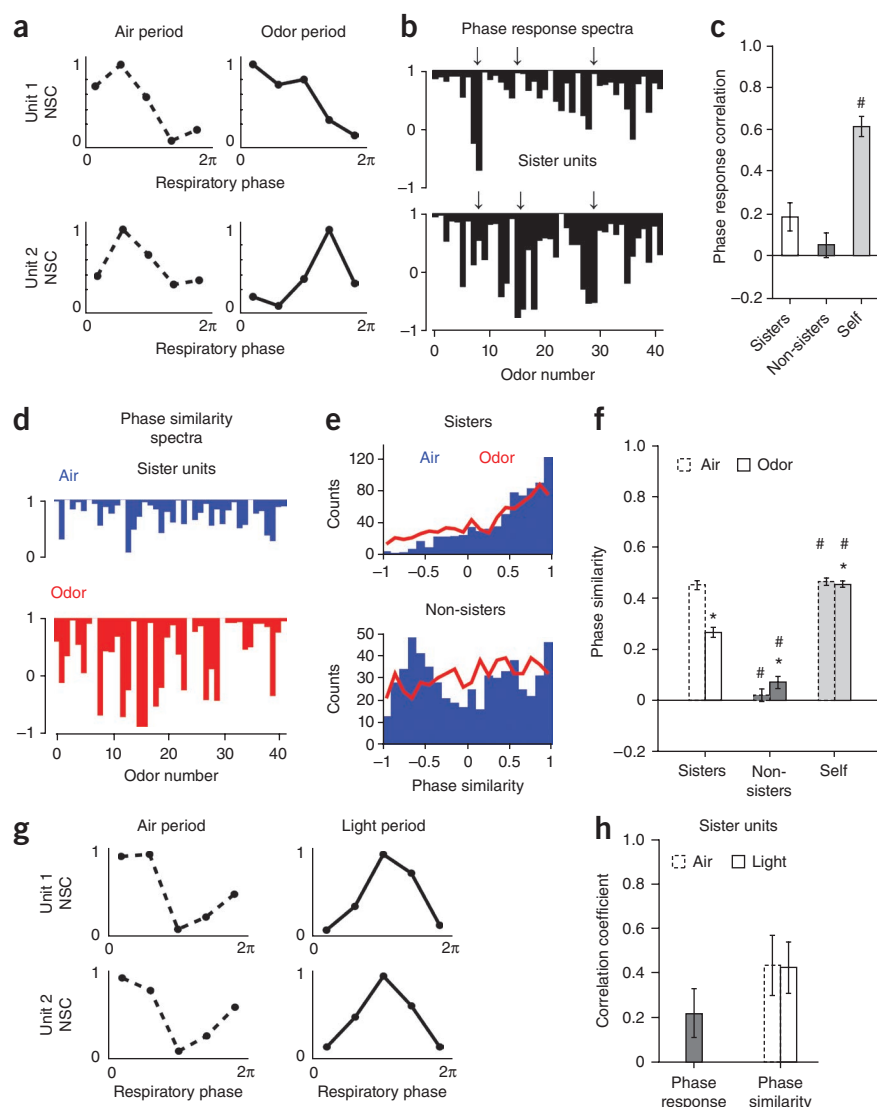


Figure 7 Odors disrupt phase correlations of sister and non-sister mitral/tufted cells. **(a)** Example phase tuning curves for two mitral/tufted units (unit 1 and unit 2) during air and odor. **(b)** Phase response spectra for one representative sister mitral/tufted unit pair. Arrows indicate example mismatches between the spectra. **(c)** Average phase response spectra correlations between sister and non-sister mitral/tufted pairs. **(d)** Example phase similarity spectra for two sister mitral/tufted cells during air (blue) and odor (red) for 42 stimuli. **(e)** Histograms of phase similarity during Air (blue) and Odor (red) for all sister ($n = 20$, top) and non-sister ($n = 15$, bottom) mitral/tufted unit pairs for 42 stimuli. **(f)** Average phase similarity for sister and non-sister mitral/tufted pairs. **(g)** Example phase tuning curves for two mitral/tufted units (unit 1 and unit 2, different from **a**) during air and light activation of single parent glomeruli. Note that light induced similar changes in phase for both units. **(h)** Left, average phase response between air and light for individual sister mitral/tufted units. Right, average phase similarity between sister mitral/tufted pairs during air (dotted line) and light (continuous line). Self refers to similarity between phase tuning curves generated from the same unit by splitting the number of trials into two. * $P < 0.05$ for comparisons within the same group (sister or non-sister mitral/tufted units) across conditions (odor versus air), # $P < 0.05$ for same condition (air or odor), across groups (sister versus non-sister mitral/tufted units) with respect to sister mitral/tufted pairs.

projection neurons, the fly analogs of sister mitral/tufted cells, fire in synchrony at rest and odor presentation triggers a further increase in spiking correlations³⁴. In experiments on the tadpole olfactory bulb³⁵, imaging activity of large populations of mitral/tufted cells using calcium-sensitive

dyes identified clusters of highly similar mitral/tufted cells that were shown in some instances to be connected to the same glomerulus. Our observation that odors desynchronize pairs of sister mitral/tufted cells is at odds with these findings from other species. Possible reasons for this include the limited numbers of odors used in these previous studies, an expanded role of local interneurons in sculpting bulbar activity patterns and the active sampling of odors by sniffing in mammals.

It is important to stress that we presented different odorants at a single nominal liquid dilution (1:100, Online Methods). It would be interesting to systematically explore the effect of odor concentration on the firing and phase properties that we have catalogued.

Origin of sister mitral/tufted cells' differential phase responses

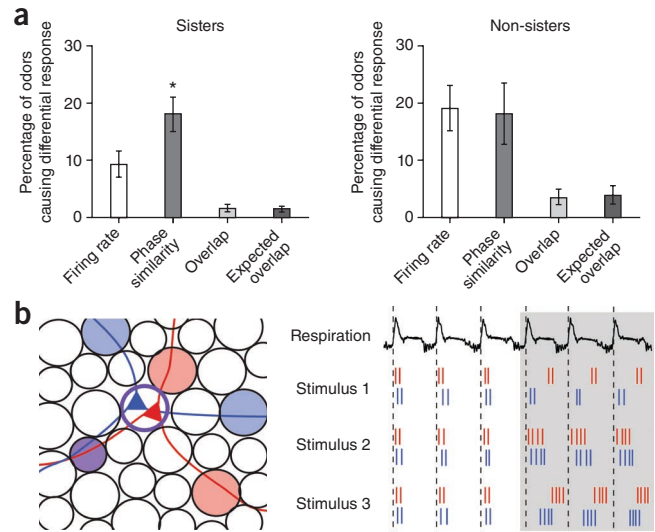
Where and how does the non-redundancy in phase properties of sister mitral/tufted cells arise? One possibility is that OSNs innervating the same glomerulus are heterogeneous in their phase responses by virtue of their spatial positioning in the olfactory epithelium³⁶. Per contra, differences in the timing of sensory axon inputs in a glomerulus have not been found³⁷. In addition, we did not observe a consistent phase relationship between sister units in terms of one cell systematically leading or lagging another (**Supplementary Fig. 4**), which would be expected if sister units received signals from spatially distinct groups

Odor response properties of sister mitral/tufted cells

In vivo studies using extracellular recordings in the olfactory bulbs of rodents came to divergent conclusions about the similarities in odor responses of neighboring mitral/tufted cells^{26,27}. This was presumably because, in contrast with our study, they could not differentiate between sister and non-sister pairs. We found that sister cells were correlated in their firing rate changes. This is consistent with the prevalent view that the glomerulus is homogenous in terms of receptor type innervation³; thus, sister cells should receive common excitatory input. *In vitro* studies have provided evidence for strong coupling between the primary dendrites of sister mitral cells, through gap junctions^{28,29} or glutamate spillover^{30,31}. Slice experiments also suggest that activation of the olfactory nerve leads to highly correlated activation of sister mitral/tufted cells^{21,32}. A recent *in vivo* study sequentially recorded from mouse mitral cells connected to the same glomerulus created by an ectopically expressed rat receptor. Consistent with our results, they found that mitral/tufted cell firing rate responses are correlated with each other and mirror presynaptic activity in their parent glomerulus³³.

Correlated firing of principal cells in the olfactory bulb or its analog brain structures appears to be a common theme across species. In the antennal lobe of *Drosophila*, genetically identified homotypic

Figure 8 Odors trigger firing rate and phase changes in an independent manner. **(a)** Average number of odors that induced differential responses in units of the same pair, considered in terms of firing rate changes or phase similarity. Overlap refers to the number of odors that induced significant changes in both firing rate and phase between units. Expected overlap refers to the number of odors that would induce significant changes in both firing rate and phase if the two were independent. Data are shown for sister (left) and non-sister (right) mitral/tufted pairs ($*P < 0.05$). **(b)** Left, cartoon representation of the diversity of sister mitral/tufted cell surround fields. Right, example spike trains of two model sister mitral/tufted cells (red and blue) during air and odor periods with respect to the respiratory cycle (top trace). Stimulus 1 elicited different phase shifts between the two neurons, but their firing rates were unchanged. Stimulus 2 elicited similar firing rate changes in both neurons and their firing times remained correlated. Stimulus 3 elicited the same firing rate change in both neurons, but different phase shifts.



of OSNs. Alternatively, differences in mitral/tufted cells intrinsic properties, such as varying spiking thresholds or differences in the expression and distribution of various ion channels, may account for the unpredictable effects of different odors on sister units. However, it is hard to envision any odor-specific effects in these scenarios. Furthermore, using light stimuli to activate only the parent glomerulus of sister units produced coordinated modulation of the phase tuning curves of sister units (Fig. 7g,h). Therefore, it is unlikely that the differences in phase properties of mitral/tufted sisters observed on odor stimulation are related to differences in intrinsic properties of the units. A circuit-level explanation seems more plausible. The phase of spiking may be influenced by the lateral input a mitral/tufted cell receives via interneurons in the glomerular layer²⁰ and/or the granule cell layer³⁸. The non-redundancy in odor responses of sister mitral/tufted cells could arise from the unique set of lateral 'surround' input connections that each cell receives. As the numbers of odors that reduce phase similarities of sister and non-sister mitral/tufted pairs are comparable (Fig. 8a), we suggest that the surrounds of sister cells are as distinct as those of non-sister cells. In our model, common input and intraglomerular interactions dominate mitral/tufted spiking at rest, leading to sister cell synchronization. Surround inhibition becomes preeminent during odor presentation because of stronger overall input to the bulb. This leads to desynchronization of preferred spiking phase of sister mitral/tufted units and further alteration of phase relationships between non-sister units.

What are the mechanisms that can uncouple firing rate changes and phase changes? One possibility is that the excitatory sensory inputs drive the overall excitability of mitral cells, whereas lateral inhibition arrives at different times³⁹, even for sister mitral/tufted cells, to sculpt the pattern of firing (Fig. 8b). This requires that sister mitral/tufted cells receive synaptic inputs from different populations of interneurons, which is plausible, but remains to be established.

Spike counts and spike timing carry independent information

A single sniff is sufficient for a rodent to distinguish closely related odors⁴⁰, thus the sniff has been thought of as representing a snapshot of the outside olfactory world. Mitral/tufted cells can convey odor information to higher brain regions by modulation of either the number of spikes in each respiratory cycle or the timing of these spikes in the cycle. The first strategy would be a form of a rate code, whereas the second would be a time code. Our finding that sister cells are similar with respect to firing rate changes, but dissimilar with respect to the timing of their spikes suggests that both types of codes may be used in an independent manner.

This implies that the mitral/tufted cells are capable of conveying different kinds of information by multiplexing rate and time codes in the same spike train.

What are these different kinds of information? Because the phase of spiking is probably influenced by the lateral input an mitral/tufted cell receives, one possibility is that the temporal code is a representation of the subset of glomeruli in the surround that are activated by the stimulus, whereas the rate code might convey the activity level of the OSNs projecting to the primary glomerulus. In other words, the temporal code may represent cross-receptor relationships that frequently differ between odors activating the same odorant receptor, whereas the rate code may be more specific to activation levels of an individual receptor that is likely to scale similarly for all odors that activate the same receptor. These two codes are largely independent (Fig. 8 and Supplementary Fig. 9).

How do downstream circuits read out the different timing of spikes? Olfactory cortical neurons are very sensitive to timing of inputs coming from mitral/tufted cells because of precisely timed feedforward inhibition^{41,42}. Therefore, sister mitral/tufted cells with different spike times may activate different populations of neurons. Other downstream brain regions that are less sensitive to timing differences may act in a more integrative mode. It will be interesting to determine whether there are such differences in bulbar target areas such as the olfactory tubercle, anterior olfactory nucleus and even the amygdala.

The non-redundancy that we found in the temporal characteristics of sister mitral/tufted cell activity suggests that many more information output channels are leaving the olfactory bulb than the number of OSN types entering it. Such an expansion of outputs suggests that the bulb is not just a relay station. On the contrary, interesting computations occur here that may be important for extracting various features from the inputs and conveying them to the cortex.

METHODS

Methods and any associated references are available in the online version of the paper at <http://www.nature.com/natureneuroscience/>.

Note: Supplementary information is available on the Nature Neuroscience website.

ACKNOWLEDGMENTS

We thank the Genome Manipulation Facility at Harvard University for help with generating the ORC mice. We are grateful to M. Meister, A. Kepecs, G. Turner, A. Khan, S. Kumari and P. Gupta for comments on the manuscript. B. Burbach,

H. Cho, R. Eifert and M. Davis provided excellent technical support. We thank G. Otazu and S. Ranade for advice on building tetrodes and H. Oviedo and A. Zador for access to the laser-scanning photostimulation rig. Our special thanks go to Megabus for swift transportation and to the House of Marks. A.K.D. and D.F.A. were supported by the Cold Spring Harbor Laboratory Fellows Program. Additional support for A.K.D. was provided by the International Society for Neurochemistry, Sarojini Damodaran fellowship (Tata Institute of Fundamental Research) and Merck.

AUTHOR CONTRIBUTIONS

A.K.D. and D.F.A. designed the study. D.F.A. engineered the ORC transgenic mice in the laboratory of V.N.M. A.H. characterized the expression pattern of ORC mice and performed acute slice recordings. A.K.D. and D.F.A. built the DLP stimulation rig and performed *in vivo* experiments. A.K.D. wrote custom software for recording and analysis. A.K.D. and D.F.A. analyzed the data. U.S.B. and V.N.M. provided expert advice on data analysis and guidance with experimental design. A.K.D., U.S.B., V.N.M. and D.F.A. wrote the manuscript.

COMPETING FINANCIAL INTERESTS

The authors declare no competing financial interests.

Published online at <http://www.nature.com/natureneuroscience/>.

Reprints and permissions information is available online at <http://www.nature.com/reprintsandpermissions/>.

- Shepherd, G.M. *The Synaptic Organization of the Brain* (Oxford University Press, New York, 1998).
- Vassar, R. *et al.* Topographic organization of sensory projections to the olfactory bulb. *Cell* **79**, 981–991 (1994).
- Mombaerts, P. Axonal wiring in the mouse olfactory system. *Annu. Rev. Cell Dev. Biol.* **22**, 713–737 (2006).
- Stewart, W.B., Kauer, J.S. & Shepherd, G.M. Functional organization of rat olfactory bulb analysed by the 2-deoxyglucose method. *J. Comp. Neurol.* **185**, 715–734 (1979).
- Rubin, B.D. & Katz, L.C. Optical imaging of odorant representations in the mammalian olfactory bulb. *Neuron* **23**, 499–511 (1999).
- Soucy, E.R., Albeanu, D.F., Fantana, A.L., Murthy, V.N. & Meister, M. Precision and diversity in an odor map on the olfactory bulb. *Nat. Neurosci.* **12**, 210–220 (2009).
- Boyden, E.S., Zhang, F., Bamberg, E., Nagel, G. & Deisseroth, K. Millisecond-timescale, genetically targeted optical control of neural activity. *Nat. Neurosci.* **8**, 1263–1268 (2005).
- Shepherd, G.M.G., Pologruto, T.A. & Svoboda, K. Circuit analysis of experience-dependent plasticity in the developing rat barrel cortex. *Neuron* **38**, 277–289 (2003).
- Royet, J.P., Souchier, C., Jourdan, F. & Ploye, H. Morphometric study of the glomerular population in the mouse olfactory bulb: numerical density and size distribution along the rostrocaudal axis. *J. Comp. Neurol.* **270**, 559–568 (1988).
- Bozza, T., McGann, J.P., Mombaerts, P. & Wachowiak, M. *In vivo* imaging of neuronal activity by targeted expression of a genetically encoded probe in the mouse. *Neuron* **42**, 9–21 (2004).
- Hartwich, K., Pollak, T. & Klausberger, T. Distinct firing patterns of identified basket and dendrite-targeting interneurons in the prefrontal cortex during hippocampal theta and local spindle oscillations. *J. Neurosci.* **29**, 9563–9574 (2009).
- Macrides, F. & Chorover, S.L. Olfactory bulb units: activity correlated with inhalation cycles and odor quality. *Science* **175**, 84–87 (1972).
- Meredith, M. Patterned response to odor in mammalian olfactory bulb: the influence of intensity. *J. Neurophysiol.* **56**, 572–597 (1986).
- Khan, A.G., Thattai, M. & Bhalla, U.S. Odor representations in the rat olfactory bulb change smoothly with morphing stimuli. *Neuron* **57**, 571–585 (2008).
- Fantana, A.L., Soucy, E.R. & Meister, M. Rat olfactory bulb mitral cells receive sparse glomerular inputs. *Neuron* **59**, 802–814 (2008).
- Kashiwadani, H., Sasaki, Y.F., Uchida, N. & Mori, K. Synchronized oscillatory discharges of mitral/tufted cells with different molecular receptive ranges in the rabbit olfactory bulb. *J. Neurophysiol.* **82**, 1786–1792 (1999).
- Mouly, A.M. & Holley, A. Perceptive properties of the multi-site electrical microstimulation of the olfactory bulb in the rat. *Behav. Brain Res.* **21**, 1–12 (1986).
- Monod, B., Mouly, A.M., Vigouroux, M. & Holley, A. An investigation of some temporal aspects of olfactory coding with the model of multi-site electrical stimulation of the olfactory bulb in the rat. *Behav. Brain Res.* **33**, 51–63 (1989).
- Arenkiel, B.R. *et al.* *In vivo* light-induced activation of neural circuitry in transgenic mice expressing channelrhodopsin-2. *Neuron* **54**, 205–218 (2007).
- Aungst, J.L. *et al.* Center-surround inhibition among olfactory bulb glomeruli. *Nature* **426**, 623–629 (2003).
- Gire, D.H. & Schoppa, N.E. Control of on/off glomerular signaling by a local GABAergic microcircuit in the olfactory bulb. *J. Neurosci.* **29**, 13454–13464 (2009).
- Engert, F., Tao, H.W., Zhang, L.I. & Poo, M. Moving visual stimuli rapidly induce direction sensitivity of developing tectal neurons. *Nature* **419**, 470–475 (2002).
- Guo, Z.V., Hart, A.C. & Ramanathan, S. Optical interrogation of neural circuits in *Caenorhabditis elegans*. *Nat. Methods* **6**, 891–896 (2009).
- Zhang, F. *et al.* Multimodal fast optical interrogation of neural circuitry. *Nature* **446**, 633–639 (2007).
- Han, X. & Boyden, E.S. Multiple-color optical activation, silencing, and desynchronization of neural activity, with single-spike temporal resolution. *PLoS ONE* **2**, e299 (2007).
- Buonviso, N. & Chaput, M.A. Response similarity to odors in olfactory bulb output cells presumed to be connected to the same glomerulus: electrophysiological study using simultaneous single-unit recordings. *J. Neurophysiol.* **63**, 447–454 (1990).
- Egaña, J.L., Aylwin, M. & Maldonado, P. Odor response properties of neighboring mitral/tufted cells in the rat olfactory bulb. *Neuroscience* **134**, 1069–1080 (2005).
- Christie, J.M. *et al.* Connexin36 mediates spike synchrony in olfactory bulb glomeruli. *Neuron* **46**, 761–772 (2005).
- Kosaka, T. & Kosaka, K. Neuronal gap junctions between intraglomerular mitral/tufted cell dendrites in the mouse main olfactory bulb. *Neurosci. Res.* **49**, 373–378 (2004).
- Nicoll, R.A. & Jahr, C.E. Self-excitation of olfactory bulb neurones. *Nature* **296**, 441–444 (1982).
- Urban, N.N. & Sakmann, B. Reciprocal intraglomerular excitation and intra- and interglomerular lateral inhibition between mouse olfactory bulb mitral cells. *J. Physiol. (Lond.)* **542**, 355–367 (2002).
- Schoppa, N.E. & Westbrook, G.L. Glomerulus-specific synchronization of mitral cells in the olfactory bulb. *Neuron* **31**, 639–651 (2001).
- Tan, J., Savigner, A., Ma, M. & Luo, M. Odor information processing by the olfactory bulb analyzed in gene-targeted mice. *Neuron* **65**, 912–926 (2010).
- Kazama, H. & Wilson, R.I. Origins of correlated activity in an olfactory circuit. *Nat. Neurosci.* **12**, 1136–1144 (2009).
- Chen, T.W., Lin, B. & Schild, D. Odor coding by modules of coherent mitral/tufted cells in the vertebrate olfactory bulb. *Proc. Natl. Acad. Sci. USA* **106**, 2401–2406 (2009).
- Miyamichi, K., Serizawa, S., Kimura, H.M. & Sakano, H. Continuous and overlapping expression domains of odorant receptor genes in the olfactory epithelium determine the dorsal/ventral positioning of glomeruli in the olfactory bulb. *J. Neurosci.* **25**, 3586–3592 (2005).
- Wachowiak, M., Denk, W. & Friedrich, R.W. Functional organization of sensory input to the olfactory bulb glomerulus analyzed by two-photon calcium imaging. *Proc. Natl. Acad. Sci. USA* **101**, 9097–9102 (2004).
- Jahr, C.E. & Nicoll, R.A. Dendrodendritic inhibition: demonstration with intracellular recording. *Science* **207**, 1473–1475 (1980).
- Kapoor, V. & Urban, N.N. Glomerulus-specific, long-latency activity in the olfactory bulb granule cell network. *J. Neurosci.* **26**, 11709–11719 (2006).
- Uchida, N. & Mainen, Z.F. Speed and accuracy of olfactory discrimination in the rat. *Nat. Neurosci.* **6**, 1224–1229 (2003).
- Luna, V.M. & Schoppa, N.E. GABAergic circuits control input-spike coupling in the piriform cortex. *J. Neurosci.* **28**, 8851–8859 (2008).
- Poo, C. & Isaacson, J.S. Odor representations in olfactory cortex: ‘sparse’ coding, global inhibition, and oscillations. *Neuron* **62**, 850–861 (2009).

ONLINE METHODS

Generating the ORC mice. Mice were engineered to express Chr2 fused to EYFP in all mature OSNs under the control of a 12-kb fragment of the rat *Omp* promoter⁴³. Two transgenic lines (#32, #33) had expression restricted to the vomeronasal organ and accessory olfactory bulb. A third line (#20, or ORC-M, used for this study) expressed Chr2-EYFP in both the olfactory epithelium and the main olfactory bulb, as well as in the vomeronasal organ and accessory olfactory bulb.

Subjects. We used a total of 89 adult ORC-M transgenic and 12 OMP-spH heterozygous mice (postnatal day 60–400, 25–55 g). Each mouse was anesthetized with a cocktail of ketamine:xylozine (initial dose of 60:6 mg per kg of body weight, intraperitoneal), attached subsequently to an anesthesia pump (Harvard Apparatus, Pump 11 Plus) and thermo regulated with a heating pad (FST TR-200). Flow of the anesthetics cocktail was kept at 40–70 $\mu\text{l h}^{-1}$ throughout a typical 12–15-h acute experiment. Low melting-point agarose (1.5%, Sigma, Type III) was poured in a thin layer above the bulb surface, after performing craniotomy and duratomy. Cortex buffer⁴⁴ was constantly circulated via a perfusion pump (ColePalmer Masterflex C/L) above the exposure. All animal procedures were performed in accordance with the guidelines of the US National Institutes of Health and were approved by the Institutional Animal Care and Use Committee at Cold Spring Harbor Laboratory.

Slice electrophysiology and light stimulation. We recorded intracellularly from mitral cells in 300- μm -thick horizontal olfactory bulb slices from postnatal day 15–30 mice, in voltage clamp mode, holding the membrane potential at -70 mV . We used $\sim 5\text{-M}\Omega$ impedance patch pipettes filled with internal solution containing cesium gluconate and Alexa 546 fluorescent dye. Laser-scanning photostimulation⁸ (DPSS Lasers, 3501–100, 354 nm, $\sim 15\text{-}\mu\text{m}$ beam diameter at the specimen) through a $4\times$ objective (Olympus, UPlanApo, NA 0.16) was used to determine the position of the parent glomerulus. An ultraviolet laser was used because it was already in operation in the experimental station for glutamate uncaging and we found that the broad excitation spectrum of Chr2 allowed for its excitation at 354 nm. Grids of 8×8 , 8×16 or 16×16 stimulation foci were superimposed onto the slice, making sure that the glomerular layer was properly sampled. We typically used 0.1–40-mW laser power (measured at the back focal plane of the objective), 1–10 ms of light stimulation and 15–150- μm inter-foci spacing. Each cell we recorded from was filled with Alexa 546 dye and imaged at $4\times$ and $60\times$ magnifications.

In vivo electrophysiology. We recorded mitral/tufted cell activity in the olfactory bulb using gold-plated tetrodes⁴⁵. Tetrodes were constructed by twisting together four 12.5- μm polyimide-coated nichrome wires (Kanthal Palm Coast) and fusing their insulation using a heat gun. To increase single unit yield, we also employed clusters of eight electrodes¹¹. These were made either by gluing together two tetrodes using Loctite 420 or by twisting together and heat-fusing eight nichrome wires. The tip of the tetrode was cut at an angle to make penetration into brain tissue easier and each electrode was gold plated to an impedance of 400–600 k Ω at 1 kHz. The electrodes were lowered into the bulb (Sutter MP-285) until they reached the dorsal mitral cell layer, characterized by the presence of multiple units with coordinated, rhythmic respiratory tuned activity at a depth of approximately 250–300 μm from the pial surface.

Electrophysiological signals were amplified 200-fold (RHA1016, Intan Technologies LLC), filtered (band pass, 300 Hz to 5 kHz), and digitized at 32 kHz (PCI-6259, National Instruments). The respiratory cycle of the mouse was recorded using piezo-electric stress transducers (RadioShack buzzer or Kent Scientific TRN0028 piezo-electric stress sensor) placed under the mouse, amplified via custom electronics and digitized in parallel with the neural signals.

In vivo light stimulation. To activate individual glomeruli in ORC mice, we used a DLP projector (Optoma EP727 or EP774) with its color wheel removed and inserted a blue filter (Edmund Industrial Optics NT52-532) in the emission path. One single lens reflex (SLR) photo lens (Nikor 50 mm, $f/1.4$, AF) was placed in front of the projector and coupled to an achromatic doublet (Thorlabs, AC508-150-A1, focal length (FL) = 150 mm) positioned so as to project the stimulus image at infinity. A second SLR photo lens (Voigtlander,

Nokton 35 mm FL, $f/1.2$) was then used to focus the image onto the bulb (Fig. 2a). One pixel of a projected image corresponded to 4 μm on the x axis and 5 μm on the y axis. A dichroic mirror (Chroma 530dcxr, round, 2-inch diameter) was used to guide blue light to the tissue. To get a timestamp of the light stimulus, we used an LED (Luxeon V, Lumileds) as a photodiode and placed it in the optical path after the first SLR lens. Two SLR lenses (the same Nokton 35 mm FL and a Nikkor 105 mm FL, $f/2.0$, AF, see Fig. 2a) coupled front to front and appended to an emission filter (Chroma, HQ510LP) were used to image the olfactory bulb onto the CCD chip of a camera (Vosskuhler 1300-QF) with a pixel size of 10 μm . Light stimuli were generally square in shape and were presented for 200 ms in 500-ms trials.

Odor stimulation. We diluted 42 odorants⁴⁶ in mineral oil (typically 1:100) and loaded them into a custom-built odor-delivery machine⁶ (Supplementary Table 1). We used a photo-ionization detector (Aurora Scientific) to determine the concentration of some of the odorants. Air was passed through Whatman filters soaked in pure odorants and subsequently diluted to calibrate the photo-ionization detector signals. The measured concentrations ranged between 0.1 to 2%. If at least two units displayed light-triggered activity in the fine-scale light mapping, the panel of odorants was serially presented to the mouse over three to five repetitions. Each trial consisted of 10 s of air followed by 5 or 10 s of odor exposure and 5 s of air. An intertrial interval of 10 or 15 s was instituted to prevent olfactory adaptation.

Spatial comparison of functional hostspots to anatomical glomeruli. Image projections from multiphoton z -stacks tessellating the bulb were stitched together using ImageJ. Blood vessel branching patterns were employed as landmarks for automated image registration using elastic deformations (bUnwarpJ⁴⁷) between the multiphoton z stack image projections and bright field images of the bulb surface. The 2DLAMs were registered first to the bright field images and the overlay onto the multiphoton images was subsequently constructed.

Counting frequency of over-stacked glomeruli. The dorsal surface of ORC-M and OMP-spH hemibulbs was sampled systematically via multiphoton microscopy. For each field of view, z stacks of the glomerular layer were obtained and the corresponding two dimensional (x - y) glomerular contours were drawn manually. Glomeruli sharing nonzero number of pixels in x - y were considered over-stacked.

Data processing. All offline analysis was carried out in MATLAB (Mathworks) and Igor Pro (Wavemetrics). Single units were identified by manual spike sorting using MClust (MClust-3.5, A.D. Redish). The sorting features used were the energy, peak height, peak to valley difference and the first two principal components of the spike waveform. The interspike interval histogram was used to test for single unit isolation, imposing the criterion that the percentage of events separated by less than 2 ms should be below 1% of the total spike interval count, indicating a well-defined refractory period.

To determine single unit cluster quality, we employed isolation distance, a commonly used metric⁴⁸. Three waveform parameters were used to compute the isolation distance: energy, peak-valley difference and the first principal component. More than 85% of the single unit clusters used had isolation distances exceeding 20, which is a standard threshold value^{49,50} (Supplementary Fig. 7).

2DLAMs were constructed by determining the average firing rate change between the stimulus and pre-stimulus periods for each spot in the grid. In these maps, each pixel represents the average change in firing rate during a 200-ms light-stimulation period for the corresponding spot on the bulb surface (Fig. 2c). A two-sample Kolmogorov-Smirnov test was used to test whether the distribution of spike counts in the 200-ms light period across repeats was significantly different ($P < 0.01$) from the spike counts in the 200-ms pre-stimulus period across all trials and repeats. If a map contained at least one significant pixel, it was subjected to further analysis.

To determine the spatial extent of the light hotspots, we selected the 2DLAMs obtained at the lowest laser intensity that still modulated activity in the recorded units. These light maps were re-sampled at 1- μm resolution by interpolation (Fig. 2c) and the hotspots fitted with two-dimensional Gaussians (Fig. 2e). The full width at half maximum (FWHM) of this two-dimensional Gaussian fit was taken as the width of the hotspot.



To quantify the magnitude of the response of a unit to a given odor, we used several metrics. First, the firing rate change (FR) induced on odor presentation was determined for each of the 42 odors to build a F-ORS.

$$FR = \frac{\text{spikes}_{\text{odor}}}{t_{\text{odor}}} - \frac{\text{spikes}_{\text{air}}}{t_{\text{air}}} \quad (1)$$

Second, to quantify changes in the cells' respiratory phase response characteristics (Fig. 4), we binned all of the spikes into five respiratory phase bins. Binning was done separately for the odor and preceding air periods, generating odor and air phase tuning curves (PTC) respectively displayed in terms of normalized spike counts (0 to 1) versus phase bin. The phase response (PR) was then defined as the correlation coefficient between the air and odor (or light) phase tuning curves.

$$PR = \text{corr}(PTC_{\text{air}}, PTC_{\text{odor}}) \quad (2)$$

The above metrics were calculated for each of the 42 odors to generate the corresponding P-ORS for each unit.

Phase similarity was used to measure similarity between the phase tuning curves of pairs of mitral/tufted cell units in both air and odor (or light) presentation periods. The Pearson correlation coefficient was calculated between the phase tuning curves of the two units for each odor (equation (4)). The same procedure was carried out on the phase tuning curves for the air period preceding odor presentation (equation (3)).

$$PS_{\text{air}} = \text{corr}(PTC_{\text{unit1,air}}, PTC_{\text{unit2,air}}) \quad (3)$$

$$PS_{\text{odor}} = \text{corr}(PTC_{\text{unit1,odor}}, PTC_{\text{unit2,odor}}) \quad (4)$$

Phase similarity values can vary from -1 to 1 : pairs of units firing at very similar phase of respiration will have values close to 1 , units that fire in opposite phases will have a value of -1 and units with no consistent relation will have values close to 0 .

To quantify trial to trial variability in spike responses of the mitral/tufted cells, we divided the odor presentation trials into two groups and applied the above mentioned metrics. This procedure gave an upper bound for measuring similarity across groups.

Firing rate changes on switching from air to odor for the two units of a pair were rescaled (FR_R) to span the same range. This range corresponded to a confidence interval spanning two s.d. (σ) about the mean firing rate change (μ) of each unit.

$$FR_R = \frac{FR - (\mu_{FR} - 2\sigma_{FR})}{4\sigma_{FR}} \quad (5)$$

An s.d.-based range was chosen to avoid outlier biases given by the maximum and minimum firing rate changes. We then performed self analysis to compute the variability across trials for each unit. We performed the same transformation on the self firing rates (FR_S).

$$\text{Rescaled } FR_S = \frac{FR_S - (\mu_{FR_S} - 2\sigma_{FR_S})}{4\sigma_{FR_S}} \quad (6)$$

We used the fluctuation in firing rate changes from trial to trial to compute a signal threshold. The threshold was picked at two s.d. of the FR_S difference distribution. Any difference in rescaled firing rate changes between the two units exceeding this threshold was classified as a differential response.

$$|\Delta FR_R| > (2\sigma_{\Delta FR_R}) \quad (7)$$

The distribution of PS_{air} for each pair of units was used to compute a signal threshold. As above, the threshold was at two s.d. from the mean PS_{air} .

$$|PS_{\text{odor}} - \mu_{PS_{\text{air}}}| > (2\sigma_{PS_{\text{air}}}) \quad (8)$$

43. Danciger, E., Mettling, C., Vidal, M., Morris, R. & Margolis, F. Olfactory marker protein gene: its structure and olfactory neuron-specific expression in transgenic mice. *Proc. Natl. Acad. Sci. USA* **86**, 8565–8569 (1989).
44. Holtmaat, A.J.G.D. *et al.* Transient and persistent dendritic spines in the neocortex *in vivo*. *Neuron* **45**, 279–291 (2005).
45. Gray, C.M., Maldonado, P.E., Wilson, M. & McNaughton, B. Tetrodes markedly improve the reliability and yield of multiple single-unit isolation from multi-unit recordings in cat striate cortex. *J. Neurosci. Methods* **63**, 43–54 (1995).
46. Adams, D. *The Hitchhiker's Guide to the Galaxy* (Pan Books, London, 1979).
47. Arganda-Carreras, I. *et al.* Consistent and elastic registration of histological sections using vector-spline regularization. *Comput. Vis. Approaches Med. Image Anal.* **4241**, 85–95 (2006).
48. Schmitzer-Torbert, N., Jackson, J., Henze, D., Harris, K. & Redish, A. Quantitative measures of cluster quality for use in extracellular recordings. *Neuroscience* **131**, 1–11 (2005).
49. Sigurdsson, T., Stark, K.L., Karayiorgou, M., Gogos, J.A. & Gordon, J.A. Impaired hippocampal-prefrontal synchrony in a genetic mouse model of schizophrenia. *Nature* **464**, 763–767 (2010).
50. Quirk, M.C., Sosulski, D.L., Feierstein, C.E., Uchida, N. & Mainen, Z.F. A defined network of fast-spiking interneurons in orbitofrontal cortex: responses to behavioral contingencies and ketamine administration. *Front. Syst. Neurosci.* **3**, 13 (2009).